MDPI

Article

Observation of a Signal Suppressing Effect in a Binary Mixture of Glycol-Water Contamination in Engine Oil with Fourier-Transform Infrared Spectroscopy

Torrey Holland [1,2], Robinson Karunanithy [1], Christopher Mandrell [1], Ali Mazin Abdul-Munaim [3], Dennis G. Watson [4] and Poopalasingam Sivakumar [1,*]

1 Department of Physics, Southern Illinois University Carbondale, 1245 Lincoln Dr, Neckers 483-A, Carbondale, IL 62901, USA
2 Department of Life and Physical Science, John A. Logan College, 700 Logan College Dr, Carterville, IL 62918, USA
3 Department of Agricultural Machines and Equipment, College of Agricultural Engineering Sciences, University of Baghdad, Baghdad 10071, Iraq
4 Department of Plant, Soil and Agricultural Systems, Southern Illinois University, Carbondale, IL 62901, USA
* Correspondence: psivakumar@siu.edu; Tel.: +1-618-453-2272

Abstract: An in-depth experimental study of the matrix effect of antifreeze (ethylene glycol) and water contamination of engine oil through FT-IR spectroscopy. With a comparison of the percent by volume concentration of contaminated fresh 15W-40 engine oil, there appeared to be a noticeable reduction in the O–H stretching signal in the infrared spectrum when ethylene glycol based antifreeze was included as a contaminant. The contaminants of distilled water, a 50/50 mixture of water and commercial ethylene glycol antifreeze, and straight ethylene glycol antifreeze were compared and a signal reduction in the O–H stretch was clearly evident when glycol was present. Doubling the volume of the 50/50 mixture as compared to water alone still resulted in a weaker O–H stretching signal. The possibility that this signal reduction was due to the larger ethylene glycol molecule having fewer O–H bonds in a given sample size was eliminated by comparing samples with the same number of O–H bonds per unit volume. The strong hydrogen bonding between that of water and glycol appeared to reduce the O–H stretching signal, even after comparing the different sample types at concentrations with the same number of O–H bonds per unit volume. Tukey's highly significant difference was used to show that samples of the 50/50 mixture and straight glycol were not reliably distinguishable from one another when comparing the same number of O–H bonds per unit volume but readily distinguishable from that of water as the lone contaminant.

Keywords: infrared spectroscopy; sonication; emulsion; glycol; antifreeze contamination; matrix effect; engine's lubrication oil

1. Introduction

Contamination of engine oil by glycol can yield severe damage to engine components within a short period [1]. While a reasonable threshold limit exists for small amounts of other harmful engine oil contamination, such as water, dirt, soot, fuel contamination, etc., in engine oil [2,3], differing sources have more caution against glycol contamination. Sources have suggested anywhere from a cautionary 200 ppm contaminate level [4], a maximum allowable value of 100 ppm [5], or having no safe limit of glycol contamination in engine lubricating oil at all [6].

Glycol-based engine coolants or antifreeze can contaminate engine oil through faulty engine seals, head gaskets, a cracked engine block, cracked cylinder heads, a defective water pump seal, or head bolts that have been improperly torqued [1,7]. When engine coolant is exposed to the engine's lubricating oil under the high heat of a running engine, the glycol

breaks down into glycolic acids that can react with metallic surfaces forming metal salts leading to corrosion or pitting [1,8] or combine with oil additives and water to form a filter plugging sludge [1,8–10]. Glycol contamination can be nearly ten times more damaging than water alone [8]. In addition, research has shown that adding TiO_2 nanoparticles to engine oil could reduce friction between components [11–15]. However, when ethylene glycol was used as a nanofluid dispersant for the TiO_2 nanoparticles in engine oil, this caused the oil to gelatinize after just 10 h of use, whereas a paraffin oil dispersant did not have the same effect and actually reduced friction between components [12,13].

To detect glycol contamination in engine oil, currently available methods include the blotter test, which simply involves placing a drop of oil on blotter paper and checking the results in a couple of hours after the oil has been well absorbed into the paper. The presence of glycol can interfere with oil dispersancy, and often a definitive black ring of soot forms around a center that is yellow or brown in color [1,8]. Another method is the Schiff's reagent test (ASTM D2982), where a sample of oil is pipetted into a solution of iodic (HIO_3) and hydrochloric (HCl) acids that oxidize glycol present in the oil, and the resulting aldehyde production turns the Schiff's reagent a pink or purple color indicating the presence of glycol [1,8,9,16]. However, the Schiff's reagent test can result in false positives with some new oils and like the blotter test, involves some subjectivity in reading the results [1,8]. Gas chromatography (ASTM 4291) has often been employed to detect glycol contamination in used engine oil, whereby water is used to help extract glycol and is centrifuged out, and the precipitates are introduced into a gas chromatographer to separate and detect the polar compounds [1,8]. A terahertz time domain spectrometer (THz-TDS) has also successfully been used to detect glycol contamination in engine oil down to the 300 ppm range [17]. Fourier-transform infrared (FT-IR) spectroscopy (ASTM E2412) has been used for a wide range of applications [18–23], and it has been commonly used to analyze engine oil in order to detect water contamination [24,25], oxidation [26], and also the absorption bands associated with glycol contamination [27], which is why it is used by several laboratories that perform oil analysis [1,8,28]. Even though ethylene glycol has four different peaks that show up in oil analysis, three of these peaks can have such strong overlap with other products potentially present in the virgin lubricant sample that one of the least prominent peaks (CH_2 rocking peak at 883 cm^{-1}) is the one used for quantification and the others are just used for verification purposes [28].

FT-IR analysis of glycol's possible intrusion into engine oil involves looking for four distinct peaks within the oil. According to the ASTM International standards, the O–H stretching that is seen with water around 3400 cm^{-1} is indicative of glycol, but glycol also has verification peaks in the ranges of 1098–1069 cm^{-1} and 1050–1030 cm^{-1} (skeletal vibration modes of the C–C and C–O stretching [10,29,30]), along with a peak used in quantification at 883 cm^{-1} (CH_2 rocking [29]) that has some overlap with diesel fuel contamination [28]. Even though the peaks centered around 1040 cm^{-1} and 1080 cm^{-1} tend to be more prominent than the peak at 883 cm^{-1}, they have such strong overlap with other products potentially present in oil that they are used for verification [28].

As previously mentioned, some tests used for glycol detection in engine oil include the blotter test, Schiff's reagent test, gas chromatography, and FT-IR analysis. However, a drawback to the previously mentioned tests is that molecular glycol needs to be present. If the glycol has already broken down in the oil, then elemental analysis can be employed to detect the telling signatures of the unique antifreeze additives left behind in the oil matrix. To that end, inductively coupled plasma spectroscopy and rotating disc electrode elemental spectroscopy are used to detect elements such as sodium, boron, and potassium within the oil that are common in antifreeze additives [1,8]. In the heated oil matrix, sodium and potassium compounds may be the most stable of the antifreeze additives but have a risk of being filtered out by the oil filter [1]. To combat this effect of causing potentially unreliably low measurements due to the filtration of the key additives, at an oil change, a piece of used oil filter can be sonicated in an ultrasonic bath of a solvent (e.g., mineral spirits or kerosene) at which point an acid digestion method may help determine the key

elements, or the subsequent residue may be filtered through a membrane and then analyzed with X-ray fluorescence spectroscopy, or the residual constituents analyzed with chemical microscopy [1].

As noted in the ASTM International standard, it states that when glycol is present within the oil, water cannot be properly quantified with FT-IR analysis, and glycol standards are prepared using a 50/50 ratio of glycol to water since this is considered the recommended ratio for most applications in coolant systems [28]. Studying this glycol/water interaction within oil would be of interest to aid in improving the quantification of the minimum level of glycol contamination.

This study explores the use of an FT-IR spectrometer to point out some of the complexities of the matrix effects of the glycol/water interaction within the oil and demonstrate the difficulties in quantifying the contaminant concentration when glycol and water both contaminate the engine oil.

2. Material and Methods

2.1. Sample Preparation

A container of a common diesel engine oil (Shell Rotella T, SAE 15W-40), a container of concentrated antifreeze (Prestone Concentrate Antifreeze/Coolant), and a container of 50/50 water to antifreeze solution (Prestone Prediluted 50/50 Antifreeze/Coolant) were purchased from a domestic retail market in Carbondale, IL, USA. A pipette was used to make different contaminated sample concentrations by volume of fresh oil with distilled water, fresh oil with concentrated antifreeze, and from fresh oil with the 50/50 premixed antifreeze solution. The treatments included different proportions of the aforementioned sample types that contaminated the fresh engine oil, as seen in Table 1a–c.

The ASTM International standard for FT-IR measurements of glycol contamination in used or in-service engine oil states that in the preparation of glycol standards, the samples need to be adequately mixed and indicate that mixing or mechanical shaking for 15 min is considered adequate [28]. It has been shown in an earlier study of creating oil standards with water contamination for FT-IR analysis that mechanical rotary mixing for two hours is still not adequate to accurately quantify the water present, even though the water standard mixing description is identical to that of glycol [25,28].

Within this study, an ultrasonic probe was employed to directly sonicate the samples to deliver high-energy mixing very quickly in order to ensure proper emulsification for clarity of IR measurements. The samples were emulsified with an ultrasonic processor (Sonic Vibra-Cell^{TM}, model: VCX750, Sonics & Materials Inc., Newtown, CT, USA) with a probe (model: CV33, Sonics & Materials, Newtown, CT, USA) diameter of 13 mm at a frequency of 20 kHz $\pm$ 50 Hz and power output of 750 W. A detailed description of the sample preparation used for this study can be found in a previous publication [24].

2.2. FT-IR Spectroscopy Analysis

The infrared spectra were recorded with an FT-IR spectrometer (Thermo-Nicolet Nexus 670, Nicolet Instrument Corporation, Madison, WI, USA) with a wavenumber range of 400 to 4000 cm^{-1}. Purging the system with dry air took place before each measurement of background or sample to minimize interference from atmospheric humidity. Potassium bromide (KBr) windows were used for their minimal infrared damping and similar index of refraction to oil, such that fringe corrections would be unnecessary, unlike with zinc selenide (ZnSe) windows [25,28]. Moreover, the KBr windows' solubility by a water/oil emulsion has a negligible effect on experimental results, more so than indeterminate errors such as sampling and instrument noise [25]. Before each sample measurement, a background measurement of the KBr windows alone was performed. From each respective sample, 3 μL was pipetted from the horizontal and vertical center of the sample vessel and dropped onto a 1-inch diameter KBr window. The same type of KBr window was used to cover the first and rotated 90 degrees to ensure an even spread of oil across both window faces. Two separate spectra measurements were recorded with 4 consecutive runs per spectrum

for each sample concentration. After spectrum acquisition of the oil emulsion, the KBr windows were cleaned using methylene chloride before procuring the next background, followed by data collection of a sample.

Table 1. (a) The three different contaminant types are listed by the total percent volume of the contaminant in the oil samples for the purposes of comparing equal volumes of the different contaminants; (b) The concentrated antifreeze and the 50/50 premixed antifreeze samples are listed by the total percent volume of the contaminant that corresponds to the percent volume of concentrated antifreeze that contaminates the oil samples for the purposes of comparing the equal amount of antifreeze concentration by different contaminants; (c) The three different contaminant types are listed by percent volume of contamination corresponding to an equal number of O–H bonds per cubic centimeter as normalized to those found in the concentrated antifreeze sample for the purposes of comparing equal amounts of O–H concentration by different contaminants. The normalization procedure is discussed in Section 2.4.

(a) Comparing equal volumes of different contaminants

Amount of Concentrated Antifreeze Contaminant (% *v/v*)	Amount of 50/50 Premixed Antifreeze/Water Contminant (% *v/v*)	Amount of Distilled Water Contaminant (% *v/v*)
0	0	0
0.1	0.1	0.1
0.2	0.2	0.2
1.0	1.0	1.0
2.0	2.0	2.0

(b) Comparing equal amount of antifreeze concentration by different contaminants

Concentration of Antifreeze by Contaminant (% *v/v*)	Amount of Concentrated Antifreeze (% *v/v*)	Amount of 50/50 Premixed Antifreeze/Water (% *v/v*)
0	0	0
0.05	0.05	0.1
0.1	0.1	0.2
0.2	0.2	0.4
1.0	1.0	2.0
2.0	2.0	4.0

(c) Comparing equal amount of O-H concentration by different contaminants

Concentration of O–H bonds in contaminant (a.u.)	Amount of Concentrated Antifreeze (% *v/v*)	Amount of 50/50 Premixed Antifreeze/Water (% *v/v*)	Amount of Distilled Water (% *v/v*)
0	0	0	0
0.5	0.5	0.244	0.161
1.0	1.0	0.487	0.322
2.0	2.0	0.975	0.645
4.0	4.0	1.95	1.289
8.21	8.21	4.0	2.646

2.3. Data Preprocessing and Analysis

Before analysis, the baselines of each spectrum were initially autocorrected using the accompanying FT-IR Omnic software (version 5.1) to minimize the effects of baseline shifting between FT-IR measurements, which can still leave some baselines shifted slightly. Thusly, where each spectrum typically lacks any detectable signals and flattens (3970 to 3995 cm^{-1}), each was shifted to zero on the absorbance scale, which was applied to the entire baseline of each respective spectrum. To enhance the signal-to-noise ratio over what is typically obtained from the equipment software, it was decided to do baseline corrections by fitting the baseline section-by-section with a polynomial function using an in-house built Python program that had also been previously reported in detail by author [31]. This

technique was utilized to avoid the baseline anomalies that can result from fitting a single polynomial over different spectral regions; however, care has to be taken to ensure that phantom baseline correction peaks do not appear where the sections of baseline corrections join. This Python-based program is a semi-automated, graphical user interface (GUI) that allows for visual confirmation of the program's ability to fit the data's baseline without anomaly, and correction parameters can be manually optimized if needed. Then, the areas used in this study were found by integration.

Comparisons of the peak areas, and in some instances, the maximum peak heights, were investigated by analysis of variance (ANOVA) [32] to determine if there was a significant difference ($\alpha = 0.05$) in absorbance among the contaminant levels by percent volume contamination (water, concentrated glycol, and a 50/50 mixture of glycol and water), by percent of glycol contamination, and by the number of O–H bonds per unit volume. Four measurements from each of the three trial replications were averaged prior to analysis, and Tukey's highly significant difference (HSD) was used to determine the differences between sample type and concentrations.

2.4. Results and Discussion

Aberrant behavior is observed within the FT-IR results of water in engine oil, glycol in engine oil, and a 50/50 mixture of water and glycol in engine oil. While some frequency shift should be expected as there is a difference between free hydrogen bonds and intramolecular hydrogen bonding [33–38], a matrix effect appears to suppress the stretching signal of the O–H functional group.

For clarity in observing the matrix effect, the number of O–H bonds of the three different mixtures have been calculated per cubic centimeter and normalized to ethylene glycol's ratio. Ethylene glycol and water essentially have the same number of O–H bonds per molecule, so a direct ratio between the two substances in moles per cubic centimeter was determined by

$$\frac{\text{water} \frac{\text{mol}}{\text{cm}^3}}{\text{ethyleneglycol} \frac{\text{mol}}{\text{cm}^3}},$$

such that the number of O–H bonds per unit volume for concentrated ethylene glycol is defined to be 1 with 1% glycol contamination, water is therefore 3.1 with 1% glycol contamination, and 50/50 glycol & water would be 4.1 with 2% 50/50 (glycol/water) contamination.

It can be seen in Figure 1 that the average spectra of a 2% contamination of a 50/50 mixture of glycol and water (1% of water and 1% of glycol) in 15W-40 engine oil has an O–H stretching peak that is less than that of 1% of water as the lone contaminant despite having the same amount of water. Even though there should be more O–H bonds in the 50/50 mixture of glycol and water exposed to the incident light, the amount of absorption around the 3400 cm^{-1} O–H peak is appreciably less than that of 1% water contamination alone. The concentrated glycol has a small signal (1% concentrated glycol in Figure 1), but due to the structure of ethylene glycol, it has less than a third of the total O–H bonds per unit volume, as does water alone. The other peaks of interest for glycol or glycol/water contamination in engine oil are the peaks of 883 cm^{-1} (CH$_2$ rocking), 1040 and 1080 cm^{-1} (C–C and C–O stretching), 1640 cm^{-1} (O–H bending). Two of the more prominent peaks in the spectra include that of 2920 cm^{-1} (CH stretching) and 1460 cm^{-1} (CH$_2$ scissoring) [39]; however, the two aforementioned peaks are independent of the contaminants, so they were not included in this study.

When plotting the maximum amplitudes for water, concentrated glycol, and the 50/50 mixture contaminants, the matrix effect is realized throughout the different concentrations, as seen in Figure 2. Here, it is noted that points on the trendline for the volume of water have a greater maximum amplitude than that of double the volume of the 50/50 antifreeze despite having an equivalent amount of water.
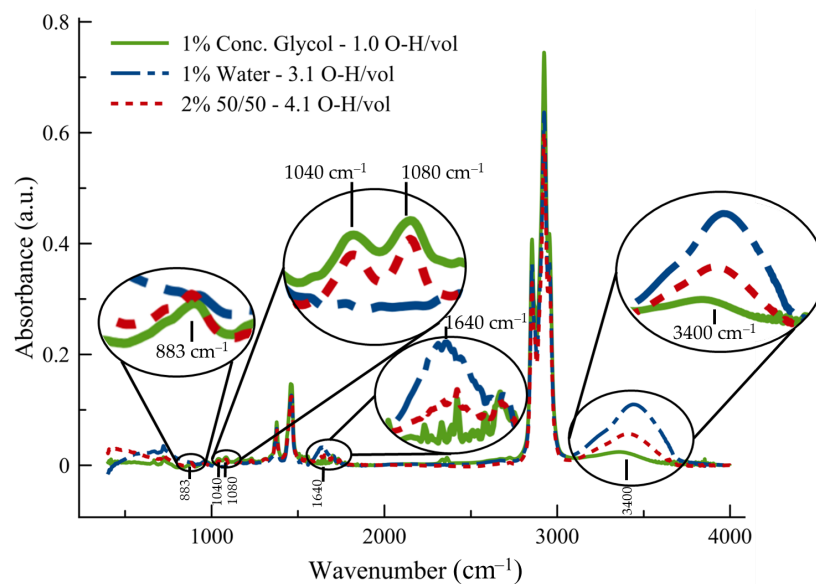
Figure 1. Typical FT-IR absorbance spectra of oil and contaminant with enlarged insets of the peaks of interest for water, glycol, and glycol/water contamination in engine oil. Note that 2% of the 50/50 mixture of glycol and water has more O–H bonds per unit volume than the other contaminants. The O–H bonds per unit volume were normalized to glycol.
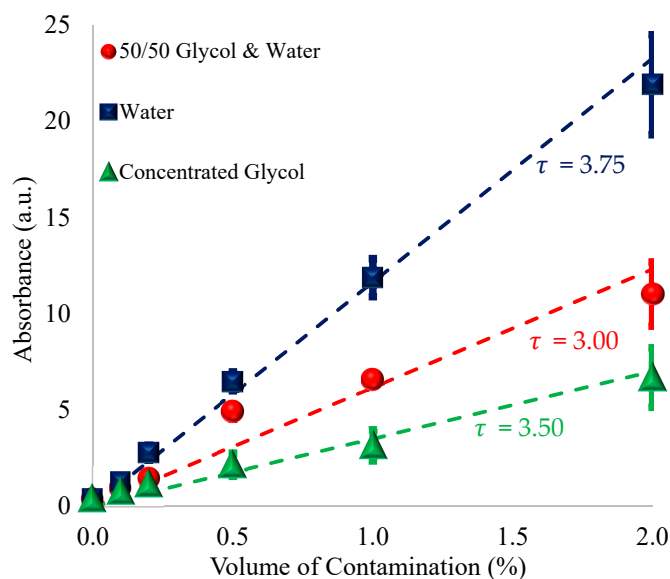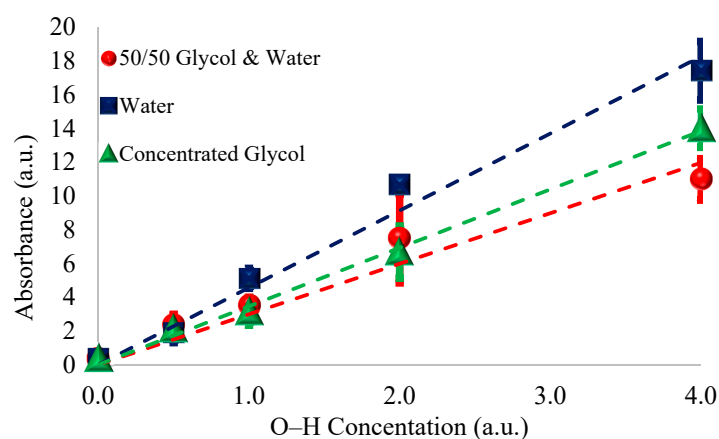

Figure 2. Average areas of absorbance of the 3400 cm^{-1} O–H peak due to contamination vs. percent concentration after emulsifying by direct probe sonication. The dashed lines represent predicted values of O–H concentration normalized to glycol as given by the normalizing constant τ, as shown on the chart, and are plotted as (O–H/vol) $* \tau$ vs. percent contamination, where the O–H per unit volume is normalized to glycol.

To illustrate this odd effect further, the absorbance of O–H is plotted as O–H concentration per unit volume in Figure 3. When plotting the O–H concentration per unit volume, the maximum measured amplitude of premixed 50/50 solution is noticeably less than that of water and even appears slightly less than that of the concentrated glycol contamination.

As the incident light interacts with the O–H bonds, the intermolecular bonds between the water molecules and glycol suppress the usual stretching of water-to-water intermolecular bonding. Ethylene glycol, $C_2H_6O_2$, is considerably more massive than a water molecule, but such critical damping of the O–H stretch lends credibility to the idea that there exists a preference of both hydrogen ends of the water molecule being bound to two separate

ethylene glycol molecules, and molecular dynamic simulations of ethylene glycol in water with molalities ranging from 1 to 5 mol/kg (~0.17% to ~0.99%) have indicated a preference for hydrogen bonding to occur between glycol and water with minimal glycol and glycol bonding [33]. Evidence supporting the preferential hydrogen bonding of a single water molecule with two glycol molecules has been noted in the past at concentrations comparable to the 50/50 ratio of glycol to water used herein with density functional theory (DFT) calculations and near-infrared studies of strictly pure ethylene glycol and water solutions undergoing incremental temperature changes from 10 °C to 90 °C [33].

Figure 3. Average areas of absorbance of the 3400 cm^{-1} O–H peak vs. O–H concentration per unit volume (normalized to glycol O–H concentration). Note that 0.0 O–H corresponds to no contamination; 0.5 O–H corresponds to 0.5% glycol, ~0.244% glycol & water, and ~0.161% water; 1.0 O–H equates to 1.0% glycol, ~0.487% glycol & water, and ~0.322% water; 2.0 O–H equates to 2.0% glycol, ~0.975% glycol & water, and ~0.645% water; and 4.0 O–H corresponds to 4.0% glycol, ~1.95% glycol & water, and ~1.289% water.

Differences between the mean of absorbance as recorded by FT-IR spectroscopy of each contamination type and concentration by percent volume of a total contaminant in the 3150–3500 cm^{-1} wavenumber range are summarized in Table 2.

Table 3 lists the differences between the areas of absorbance in the total glycol contamination, where, for example, a percent glycol contamination of 0.5% in the table, depending on the respective row header, implies that the total percent of contaminant used was either a total contamination of 0.5% of the concentrated glycol or a 1.0% total contamination of the premixed glycol/water contaminant (only half of that actually being glycol).

Tables 2 and 3 confirm the similar behavior of O–H peaks (3150–3500 cm^{-1}) with the mean area under the curve and the mean amplitude data analysis; thus, the rest of the data analysis uses the area under the curve. The differences between the areas of absorbance in the O–H bonds per unit volume for the three types of contaminants are summarized in Table 4, where an O–H contamination is normalized to that of the concentrated glycol such that an O–H rate of 0.5 corresponds to 0.5% straight glycol, ~0.244% glycol/water, and ~0.161% distilled water.

Table 2. Summary of the differences in contamination levels of the mean absorbance in the 3150–3500 cm^{-1} wavenumber range.

		Percent Contamination					
		0.0%	0.1%	0.2%	0.5%	1.0%	2.0%
Contaminant Type	N	Mean *	Mean *	Mean *	Mean *	Mean *	Mean *
Water	3	0.0011369 a	0.0038145 a	0.0085823 a	0.0194665 a	0.037366 a	0.063110 a
Glycol/Water	3	0.0011369 a	0.0029290 a	0.0037119 b	0.0141760 b	0.018696 b	0.033128 b
Glycol	3	0.0011369 a	0.0025882 a	0.0037100 b	0.0068265 c	0.009768 c	0.018479 c

* Means in the same column with the same letter are not significantly different.

Table 3. Summary of the differences in contamination levels of the mean absorbance area in the 3150–3500 cm^{-1} wavenumber range.

| Contaminant Type | N | Percent Glycol Contamination | | | | | | |
| | | 0.0% | 0.05% | 0.1% | 0.2% | 0.5% | 1.0% | 2.0% |
		Mean *	Mean *	Mean *	Mean *	Mean *	Mean *	Mean *
Glycol/Water	3	0.39452 a	1.0167 a	1.2892 a	3.1154 a	6.5002 a	11.518 a	21.1346 a
Glycol	3	0.39452 a	0.8295 a	0.8969 a	1.2906 b	2.3758 b	3.401 b	6.4343 b

* Means in the same column with the same letter are not significantly different.

Table 4. Summary of the differences in O–H contamination rates as measured by the mean absorbance in the area of the 3150–3500 wavenumber range. The % *v/v* equivalents for each contaminant type are shown for the corresponding O–H contamination rate.

| Contaminant Type | N | O–H Contamination | | | | | | | | | | | |
| | | 0.0 | | 0.5 | | 1.0 | | 2.0 | | 4.0 | | 8.21 | |
		Mean *	% *v/v*	Mean *	% *v/v*	Mean *	% *v/v*	Mean *	% *v/v*	Mean *	% *v/v*	Mean *	% *v/v*
Water	3	0.39452 a	0.0	1.9365 a	0.161	5.1416 a	0.322	10.684 a	0.645	17.446 a	1.289	28.897 a	2.646
Glycol/Water	3	0.39452 a	0.0	2.3748 a	0.244	3.5487 b	0.487	7.497 ab	0.975	11.055 b	1.95	21.135 b	4.0
Glycol	3	0.39452 a	0.0	2.3758 a	0.5	3.4007 b	1.0	6.434 b	2.0	13.623 b	4.0	24.527 ab	8.21

* Means in the same column with the same letter are not significantly different.

From Table 4, it is possible to distinguish O–H contamination due to water from that of glycol or due to water from that of a 50/50 glycol/water contamination with FT-IR for all concentrations of contaminants except for 0.5 O–H a.u. However, the FT-IR was not capable of reliably distinguishing between the O–H contaminations due to glycol and glycol/water, but some distinctions appear between the two at the O–H concentrations of 2.0 (2% glycol and ~0.975% glycol/water) and 8.21 (8.21% glycol and 4% glycol/water). Furthermore, the mean area of the O–H peak switches from being glycol/water dominant to glycol dominant. As noted in a previous study, the linear behavior and steepest increasing slope observed for increasing water contaminations in 15W-40 engine oil are less than 2% contamination [25]. Water's gradually diminishing effect on the increase in the O–H peak above 2% contamination could be partially responsible for this inversion; however, it requires further systematic investigation with DFT calculations of increasing concentrations of water in a medium of a large hydrocarbon chain with supplemental additions of known oil additives, such as detergents and demulsifiers.

3. Conclusions

This work supports the previous, theoretically established evidence from molecular dynamic simulations (~0.17% to ~0.99% ethylene glycol in water) [33] and DFT calculations with near-infrared analyses of 5%, 50%, & 95% ethylene glycol in water [36] that the intermolecular bonds of ethylene glycol molecules are quite strong and that the bond between ethylene glycol and water is more substantial than a water-to-water bond, making it the preferential bonding type if there exits enough glycol for two molecules to "tie up" each water molecule. Here, it is established that this may suppress the O–H stretching signal in infrared spectroscopy investigations of antifreeze contaminated engine oil and can generate potentially misleading results on the actual concentrations of contamination.

Due to the O–H signal's suppression being so great that even when accounting for the same number of O–H bonds per unit volume, the 50/50 mixture and the concentrated glycol contaminants are readily distinguishable from water as the sole contaminant but not readily distinguishable from one another. Further investigations could include DFT-based molecular dynamic calculations of glycol and water at different ratios in a medium of a large hydrocarbon chain, such as is found in base engine oil, to look at the spatially depen-

dent electron densities within the given electronic structure in order to deduce the likely intermolecular and intramolecular bonding interactions at play. The approximations used in DFT calculations still require experimental confirmation [40], and to that end, changing the ratio of glycol concentrations to water could more effectively reveal this matrix effect as water content increases, forcing water-to-water bonds within the glycol matrix, perhaps reducing the suppression of the O–H signal. Creating a calibration curve could be useful in allowing better water quantification in the presence of glycol as determined by another glycol peak (883 cm^{-1}). The confirmation and quantification of current levels of glycol contamination in a sample could lead to a better assessment of water concentration. Since the water content in the presence of glycol points to a coolant leak, which typically starts out as 50/50 antifreeze, then a better estimation of the minimum total glycol contamination may be performed despite the rapid decomposition of glycol in oil at typical engine operating temperatures.

Author Contributions: P.S. and T.H. initiated the research idea, P.S., T.H. and D.G.W. designed the experiment, T.H. and R.K. performed the experiments, and T.H., P.S., R.K., C.M., A.M.A.-M. and D.G.W. analyzed the data and wrote the paper. All authors have read and agreed to the published version of the manuscript.

Institutional Review Board Statement: Not applicable.

Informed Consent Statement: Not applicable.

Data Availability Statement: Not applicable.

Conflicts of Interest: The authors declare no conflict of interest.

References

1. Fitch, J.; Corporation, N. Glycol in Lubricating Oil-Detection, Analysis and Removal. *Mach. Lubr.* **2014**, *15*, 1–9.
2. Pawlak, Z.B.T.-T. (Ed.) *Chapter 6-Analytical Techniques in Lubricating Practices. Tribochemistry Lubr. Oils*; Elsevier: Amsterdam, The Netherlands, 2003; Volume 45, pp. 217–265. [CrossRef]
3. Salehi, F.M.; Morina, A.; Neville, A. The effect of soot and diesel contamination on wear and friction of engine oil pump. *Tribol. Int.* **2017**, *115*, 285–296. [CrossRef]
4. Angeles, R. Tables on Oil Analysis 2003. Available online: https://www.rsareliability.com/Oil%20Analysis%20Tables.pdf (accessed on 1 June 2018).
5. MTU Friedrichshafen GmbH. Fluids and Lubricants Specifications 2012; pp. 1–135. Available online: https://authorzilla.com/zG2rD/fluids-and-lubricants-specifications-mtu.html (accessed on 5 June 2018).
6. Van Rensselar, J. Used Oil Condemning Limits. *Tribol. Lubr. Technol.* **2012**, *68*, 36–43.
7. Raţiu, S.; Josan, A.; Alexa, V.; Cioată, V.G.; Kiss, I. Impact of contaminants on engine oil: A review. *J. Phys. Conf. Ser.* **2021**, *1781*, 012051. [CrossRef]
8. Scientific Spectro. *Guide to Measuring Glycol Contamination in Oil*; Spectro Sci.: Chelmsford, MA, USA, 2016; pp. 1–5.
9. Agarwal, A.K. Lubricating Oil Tribology of a Biodiesel-Fuelled Compression Ignition Engine. In Proceedings of the ASME 2003 Internal Combustion Engine Division Spring Technical Conference, Salzburg, Austria, 11–14 May 2003; pp. 751–765. [CrossRef]
10. Hönig, V.; Procházka, P.; Obergruber, M.; Kučerová, V.; Mejstřík, P.; Macků, J.; Bouček, J. Determination of Tractor Engine Oil Change Interval Based on Material Properties. *Materials* **2020**, *13*, 5403. [CrossRef]
11. Suryawanshi, S.; Pattiwar, J. Effect of TiO$_2$ Nanoparticles Blended with Lubricating Oil on the Tribological Performance of the Journal Bearing. *Tribol. Ind.* **2018**, *40*, 370–391. [CrossRef]
12. Wu, Y.; Kao, M. Using TiO$_2$ nanofluid additive for engine lubrication oil. *Ind. Lubr. Tribol.* **2011**, *63*, 440–445. [CrossRef]
13. Kumar, M.; Afzal, A.; Ramis, M.K. Investigation of physicochemical and tribological properties of TiO$_2$ nano-lubricant oil of different concentrations. *Tribologia* **2017**, *35*, 6–15.
14. Laad, M.; Jatti, V.K.S. Titanium oxide nanoparticles as additives in engine oil. *J. King Saud Univ.-Eng. Sci.* **2018**, *30*, 116–122. [CrossRef]
15. Ilie, F.; Covaliu, C. Tribological Properties of the Lubricant Containing Titanium Dioxide Nanoparticles as an Additive. *Lubricants* **2016**, *4*, 12. [CrossRef]
16. Lister, T. *Industrial Chemistry Case Studies: Industrial Processes in the 1990s*, 1st ed.; Royal Society of Chemistry: London, UK, 1999.
17. Abdulmunem, O.M.; Abdul-Munaim, A.M.; Aller, M.M.; Preu, S.; Watson, D.G. THz-TDS for Detecting Glycol Contamination in Engine Oil. *Appl. Sci.* **2020**, *10*, 3738. [CrossRef]

18. Karunanithy, R.; Holland, T.; Sivakumar, P. Influence of Glutaraldehyde's Molecular Transformations on Spectroscopic Investigations of Its Conjugation with Amine-Modified Fe_3O_4 Microparticles in the Reaction Medium. *Langmuir* **2021**, *37*, 5242–5251. [CrossRef]

19. Berthomieu, C.; Hienerwadel, R. Fourier transform infrared (FTIR) spectroscopy. *Photosynth. Res.* **2009**, *101*, 157–170. [CrossRef]

20. Ami, D.; Mereghetti, P.; Leri, M.; Giorgetti, S.; Natalello, A.; Doglia, S.M.; Stefani, M.; Bucciantini, M. A FTIR microspectroscopy study of the structural and biochemical perturbations induced by natively folded and aggregated transthyretin in HL-1 cardiomyocytes. *Sci. Rep.* **2018**, *8*, 1–15. [CrossRef]

21. Breton, J. Fourier transform infrared spectroscopy of primary electron donors in type I photosynthetic reaction centers. *Biochim. Biophys. Acta* **2001**, *1507*, 180–193. [CrossRef]

22. Guang, P.; Huang, W.; Guo, L.; Yang, X.; Huang, F.; Yang, M.; Wen, W.; Li, L. Blood-based FTIR-ATR spectroscopy coupled with extreme gradient boosting for the diagnosis of type 2 diabetes: A STARD compliant diagnosis research. *Medicine* **2020**, *99*, 1–7. [CrossRef]

23. Tambe, E.; Gotmare, S. Ftir Analysis and Interpretation of Ir Spectra of Four Spice Oils Extracted By Hydrodistillation. *World J. Pharm. Pharm. Sci.* **2022**, *11*, 1346–1363. [CrossRef]

24. Holland, T.; Abdul-Munaim, A.M.; Watson, D.G.; Sivakumar, P. Influence of Sample Mixing Techniques on Engine Oil Contamination Analysis by Infrared Spectroscopy. *Lubricants* **2019**, *7*, 4. [CrossRef]

25. Holland, T.; Abdul-Munaim, A.M.; Watson, D.G.; Sivakumar, P. Importance of Emulsification in Calibrating Infrared Spectroscopes for Analyzing Water Contamination in Used or In-Service Engine Oil. *Lubricants* **2018**, *6*, 35. [CrossRef]

26. Abdul-Munaim, A.M.; Holland, T.; Sivakumar, P.; Watson, D.G. Absorption Wavebands for Discriminating Oxidation Time of Engine Oil as Detected by FT-IR Spectroscopy. *Lubricants* **2019**, *7*, 24. [CrossRef]

27. Holland, T.; Karunanithy, R.; Abdul-Munaim, A.M.; Mandrell, C.; Watson, D.G.; Sivakumar, P. P3412 Determination of Glycol Contamination in Engine Oil by Infrared and UV-Vis Spectroscopy. In Proceedings of the 73rd International Symposium on Molecular Spectroscopy, Champaign, IL, USA, 18–22 June 2018.

28. ASTM International. *ASTM E2412-10*; Standard Practice for Condition Monitoring of Used Lubricants by Trend Analysis Using Fourier Transform Infrared (FT-IR) Spectrometry. ASTM International: West Conshohocken, PA, USA, 2010; pp. 1–22. [CrossRef]

29. Guo, Y.-C.; Cai, C.; Zhang, Y.-H. Observation of conformational changes in ethylene glycol–water complexes by FTIR–ATR spectroscopy and computational studies. *AIP Adv.* **2018**, *8*, 055308. [CrossRef]

30. Buckley, P.; Giguère, P.A. Infrared studies on rotational isomerism. I. Ethylene glycol. *Can. J. Chem.* **1967**, *45*, 397–407. [CrossRef]

31. Mandrell, C.T.; Holland, T.E.; Wheeler, J.F.; Esmaeili, S.M.A.; Amar, K.; Chowdhury, F.; Sivakumar, P. Machine Learning Approach to Raman Spectrum Analysis of MIA PaCa-2 Pancreatic Cancer Tumor Repopulating Cells for Classification and Feature Analysis. *Life* **2020**, *10*, 181. [CrossRef]

32. Holland, T.; Abdul-Munaim, A.M.; Mandrell, C.; Karunanithy, R.; Watson, D.G.; Sivakumar, P. UV-Visible Spectrophotometer for Distinguishing Oxidation Time of Engine Oil. *Lubricants* **2021**, *9*, 37. [CrossRef]

33. Weng, L.; Chen, C.; Zuo, J.; Li, W. Molecular Dynamics Study of Effects of Temperature and Concentration on Hydrogen-Bond Abilities of Ethylene Glycol and Glycerol: Implications for Cryopreservation. *J. Phys. Chem. A* **2011**, *115*, 4729–4737. [CrossRef]

34. Ma, X.; Wang, J. Differentiating Subtle Variation of Weak Intramolecular Hydrogen Bond in Vicinal Diols by Linear Infrared Spectroscopy. *J. Phys. Chem. A* **2009**, *113*, 6070–6076. [CrossRef]

35. Ma, X.; Cai, K.; Wang, J. Dynamical Structures of Glycol and Ethanedithiol Examined by Infrared Spectroscopy, Ab Initio Computation, and Molecular Dynamics Simulations. *J. Phys. Chem. B* **2011**, *115*, 1175–1187. [CrossRef]

36. Chen, Y.; Ozaki, Y.; Czarnecki, M.A. Molecular structure and hydrogen bonding in pure liquid ethylene glycol and ethylene glycol–water mixtures studied using NIR spectroscopy. *Phys. Chem. Chem. Phys.* **2013**, *15*, 18694–18701. [CrossRef]

37. Howard, D.L.; Jørgensen, P.; Kjaergaard, H.G. Weak Intramolecular Interactions in Ethylene Glycol Identified by Vapor Phase OH−Stretching Overtone Spectroscopy. *J. Am. Chem. Soc.* **2005**, *127*, 17096–17103. [CrossRef]

38. Kaiser, A.; Ritter, M.; Nazmutdinov, R.; Probst, M. Hydrogen Bonding and Dielectric Spectra of Ethylene Glycol–Water Mixtures from Molecular Dynamics Simulations. *J. Phys. Chem. B* **2016**, *120*, 10515–10523. [CrossRef]

39. Rahimi, B.; Semnani, A.; Nezamzadeh-Ejhieh, A.; Shakoori Langeroodi, H.S.; Davood, M.H. Monitoring of the Physical and Chemical Properties of a Gasoline Engine Oil during Its Usage. *J. Anal. Methods Chem.* **2012**, *2012*, 819524. [CrossRef]

40. Van Mourik, T.; Bühl, M.; Gaigeot, M.-P. Density functional theory across chemistry, physics and biology. *Philos. Trans. R. Soc. London. Ser. A Math. Phys. Eng. Sci.* **2014**, *372*, 20120488. [CrossRef]